Electronic Supplementary Information (ESI)

Photocatalytic oxidation of iron(II) complexes by dioxygen with 9-mesityl-10-methylacridinium ion

Takeshi Tsudaka,[a] Kei Ohkubo[*ab] and Shunichi Fukuzumi[*abc]

[a] *Department of Material and Life Science, Graduate School of Engineering, Osaka University, ALCA and SENTAN, Japan Science and Technology Agency (JST), Suita, Osaka 565-0871, Japan. E-mail: fukuzumi@chem.eng.osaka-u.ac.jp; Fax: +81-6-6879-7370*

[b] *Department of Chemistry and Nano Science, Ewha Womans University, Seoul 120-750, Korea.*

[c] *Faculty of Science and Technology, Meijo University, ALCA and SENTAN, Japan Science and Technology Agency (JST), Nagoya, Aichi 468-8502, Japan*

E-mail: ookubo@chem.eng.osaka-u.ac.jp
fukuzumi@chem.eng.osaka-u.ac.jp

Experimental Section

Materials. All chemicals commercially available were used without further purification unless otherwise noted. 4,4'-dimethyl-2,2'-bipyridyl was supplied by Aldrich Chemicals. $FeSO_4•7H_2O$, 2,2'-bipyridyl, NH_4PF_6, hydrochloric acid (35%) were purchased from Wako Pure Chemical Industries Ltd. 9-Mesityl-10-methylacridinium perchlorate (Acr^+–Mes), trifluoromethanesulfonic acid, $Ce(NH_4)_2(NO_3)_6$, oxo[5,10,15,20-tetra(4-pyridyl)porphinato]titanium(IV) ([TiO(tpyp)]), 5-chlorophenanthroline, 1,1'-dibromoferrocene and bromoferrocene were supplied by Tokyo Chemical Industry Co., Ltd. (TCI). Purification of water (18.2 MΩ•cm) was performed with a Milli-Q system (Millipore, Direct-Q 3 UV). 9-Mesityl-10-methyl acridinium ion (Acr^+–Mes) was purified by recrystallization from methanol. Acetonitrile (MeCN) used as solvent was purified and dried by the standard procedure.[S1] 10-Methyl-9,10-dihydroacridine was synthesized according to the published procedure.[S2] $[Fe^{II}(bpy)_3]^{2+}(PF_6^-)_2$, $[Fe^{II}(Clphen)_3]^{2+}(PF_6^-)_2$, $[Fe^{II}(Me_2bpy)_3]^{2+}(PF_6^-)_2$ were synthesized according to the published procedure.[S3]

Reaction Procedure. The photocatalytic oxidations of $[Fe^{II}(bpy)_3]^{2+}$ were examined by monitoring UV−vis spectral changes using a Hewlett-Packard HP8453 diode array spectrophotometer under irradiation with a xenon lamp (Ushio Optical ModelX SX-UID 500XAMQ) through a colour filter glass (Asahi Techno Glass Y43) transmitting $\lambda > 390$ nm at 298 K. Typically, a dehydrated MeCN solution (0.40 mL) of $[Fe^{II}(bpy)_3]^{2+}(PF_6^-)_2$ (2.0×10^{-3} M) containing Acr^+–Mes (2.0×10^{-4} M) and HOTf (0.10 M) in a square quartz cell (total vol. 0.40 mL) sealed with a rubber septum saturated by bubbling with oxygen for 10 min. Oxidation reactions of iron(II) complexes were monitored by the decrease in the absorption band due to $[Fe^{II}(bpy)_3]^{2+}$ derivatives ($[Fe^{II}(bpy)_3]^{2+}$: λ_{max} = 522 nm, ε_{max} = 8.65×10^3 M^{-1} cm^{-1}, $[Fe^{II}(Me_2bpy)_3]^{2+}$: λ_{max} = 528 nm, ε_{max} = 9.25×10^3 M^{-1} cm^{-1}, $[Fe^{II}(Clphen)_3]^{2+}$: λ_{max} = 510 nm, ε_{max} = 1.11×10^4 M^{-1} cm^{-1}) or the rise in the absorption band due to ferrocenium ions ($[Fe^{III}(BrC_5H_4)_2]^+$: λ_{max} = 675 nm, ε_{max} = 280 M^{-1} cm^{-1}, $[Fe^{III}(BrC_5H_4)(C_5H_5)]^+$: λ_{max} = 706 nm, ε_{max} = 330 M^{-1} cm^{-1}). Formation of iron(III) complexes was confirmed by addition of MeCN solution containing 10-Methyl-9,10-dihydroacridine. The amount of iron(III) complexes contained the fraction contributed to oxidation by hydrogen peroxide. The photocatalytic oxidation by using $QuPh^+$–NA as photocatalyst undergo the same conditions except for irradiation with a xenon lamp through a colour

filter glass transmitting $\lambda > 300$ nm. The amount of hydrogen peroxide was determined by spectroscopic titration with an acidic solution of $[TiO(tpypH_4)]^{4+}$ complex (Ti-TPyP reagent). The Ti-TPyP complex was prepared by dissolving 3.4 mg of the Ti-TPyP complex in 100 mL of 50 mM hydrochloric acid. 0.10 mL of reaction solution was diluted by 0.10 mL of water. To 0.20 mL of the diluted sample, 0.20 mL of 4.8 M perchloric acid and 0.20 mL of the Ti-TPyP reagent were added. The mixed solution was stirred for 30 sec. This sample solution was diluted to 2.0 mL with water and used for the spectroscopic measurement. The absorbance at $\lambda = 434$ nm was measured using a Hewlett Packard 8453 diode array spectrophotometer (A_S) A blank solution was prepared in a similar manner by adding water instead of the sample solution in the same volume with its absorbance designated as follows: $\Delta A_{434} = A_B - A_S$. Based on ΔA_{434} and the volume of the solution, the amount of hydrogen peroxide was determined according to the literature. [S4]

Quantum yield measurements. The quantum yield (QY) was

$$\text{QY}\ (\%) = \frac{R}{I \times A(1 - 10^{-A_{tot}})/A_{tot}} \times 100$$

estimated as where R (mol s^{-1}) represents the formation rate of iron(III) complexes, I coefficient (einstein s^{-1}) based on the rate of the number of incident photons, and $A(1 - 10^{-A_{tot}})/A_{tot}$ represents calculated absorbed fraction contributed to the photocatalyst due to overlapping of the photocatalyst and the iron complex. A standard actinometer (potassium ferrioxalate) was used for the quantum yield determination of the photooxidation of $[Fe^{II}(bpy)_3]^{2+}$ and its derivatives. A quartz cuvette (0.10 cm) which contained a MeCN solution (0.40 mL) of Acr^+–Mes (1.0×10^{-3} M), $[Fe^{II}(bpy)_3]^{2+}(PF_6^-)_2$ (5.0×10^{-4} – 2.0×10^{-3} M) and HOTf (0.15 M) was irradiated with monochromatized light of $\lambda = 420$ nm from a Shimadzu RF-5300PC fluorescence spectrophotometer. The light intensity of monochromatized light of $\lambda = 420$ nm was determined as 2.3×10^{-8} einstein s^{-1} with an illumination bandwidth of 20 nm. $QuPh^+$–NA, instead of Acr^+–Mes as the photocatalyst, was irradiated with the light of $\lambda = 335$ nm (light intensity: 1.6×10^{-8} einstein s^{-1}). Using ferrocene derivatives, a quartz cuvette (0.10 cm) which contained a MeCN solution (3.0 mL) of Acr^+–Mes (1.0×10^{-3} M), $Fe^{II}(BrC_5H_4)(C_5H_5)$ (2.0×10^{-4} – 1.0×10^{-3} M) and HOTf (0.15 M) was irradiated with monochromatized light of $\lambda = 420$ nm (light intensity: 7.2×10^{-9} einstein s^{-1}). $QuPh^+$–NA was irradiated with the light of $\lambda = 335$ nm (light intensity: 5.1×10^{-9}

einstein s^{-1}). The photochemical reaction was monitored by using a Hewlett-Packard 8453 photodiode array spectrophotometer. The amount of iron(III) complexes was determined from a decrease in absorbance due to $[Fe^{II}(bpy)_3]^{2+}$ derivatives or the rise in the absorption band due to ferrocenium ion. The mixed gas was controlled by using a gas mixer (Kofloc GB-3C, KOJIMA Instrument Inc.), which can mix two or more gases at a certain pressure and flow rate.

Laser Flash Photolysis.

An N_2-saturated MeCN solution containing $[Fe^{II}(bpy)_3]^{2+}(PF_6^-)_2$ ($2.7 \times 10^{-5} – 1.0 \times 10^{-4}$ M) and photocatalyst (1.0×10^{-4} M) was excited by a Panther OPO pumped by Nd:YAG laser (Continuum, SLII-10, 4-6 ns fwhm) at λ = 355 nm with a power of 10 mJ per pulse. The transient absorption measurements were performed using a continuous xenon lamp (150 W) and an InGaAsPIN photodiode (Hamamatsu 2949) as a probe light and a detector, respectively. The output from the photodiodes and a photomultiplier tube was recorded with a digitizing oscilloscope (Tektronix, TDS3032, 300 MHz). The transient spectra were recorded using fresh solutions in each laser excitation at 298 K.

S1. W. L. F. Armarego and C. L. L. Chai, *Purification of Laboratory Chemicals*, 6th ed., Butterworth-Heinemann, Amsterdam, 2009.

S2. (a) R. M. G. Roberts, D. Ostovic and M. M. Kreevoy, *Faraday Discuss. Chem. Soc.,* 1982, **74**, 257. (b) S. Fukuzumi, Y. Tokuda, T. Etano, T. Okamoto and J. Otera, *J. Am. Chem. Soc.,* 1993*,* **115***,* 8960.

S3. P. S. Braterman, J. I. Song and R. D. Peacock, *Inorg. Chem*., 1992, **31**, 555.

S4. C. Matsubara, N. Kawamoto and K. Takamura, *Analyst,* 1992, **117**, 1781.

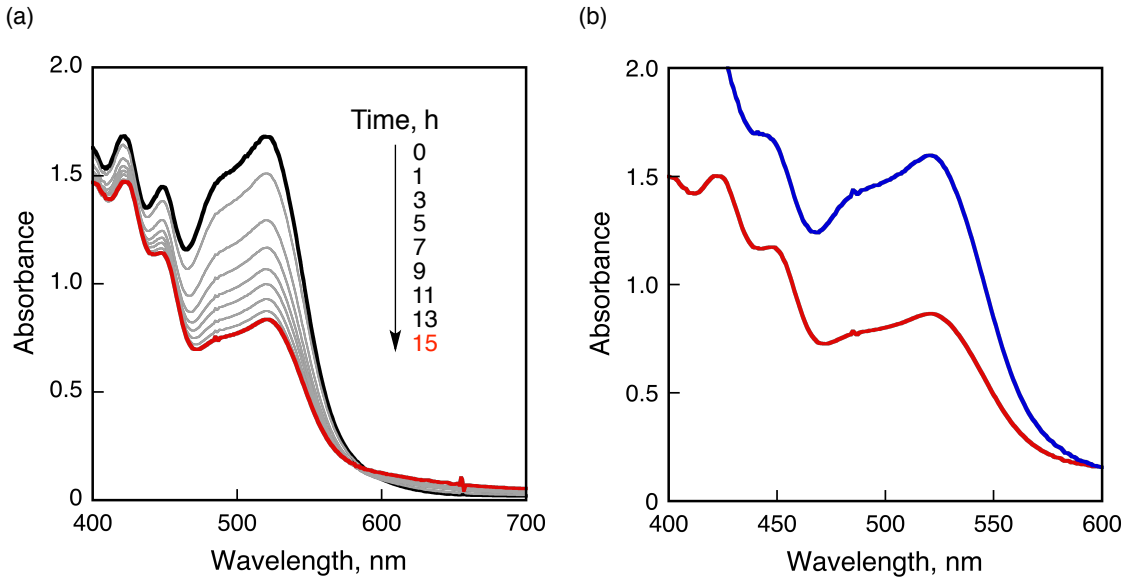

Fig. S1 (a) Visible absorption changes in oxidation of $[Fe^{II}(bpy)_3]^{2+}(PF_6^-)_2$ (2.0×10^{-4} M) by O_2 in O_2-saturated acetonitrile containing HOTf (5.0×10^{-2} M) in the presence of $[Acr^+–Mes](ClO_4^-)$ (2.0×10^{-4} M) at 298 K under visible light irradiation using a xenon lamp with a cut filter ($\lambda > 390$ nm) for 0 h (black line) and 15 h (red line). (b) Absorption spectral change before (red line) and after (blue line) addition of 9,10-dihydro-10-methylacridine (1.0×10^{-2} M) to reaction solution after visible light irradiation for 15 h

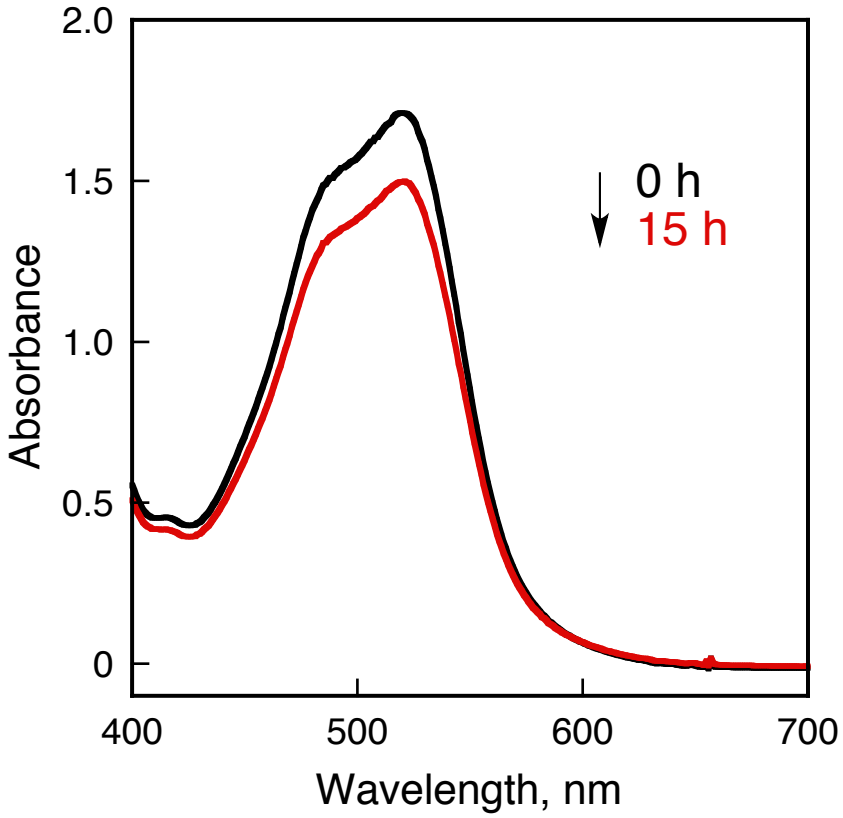

s

Fig. S2 Visible absorption changes in oxidation of $[Fe^{II}(bpy)_3]^{2+}(PF_6^-)_2$ (2.0×10^{-4} M) by O_2 in O_2-saturated acetonitrile containing HOTf (5.0×10^{-2} M) at 298 K under visible light irradiation using a xenon lamp with a cut filter ($\lambda >$ 390 nm) for 0 h (black line) and 15 h (red line).

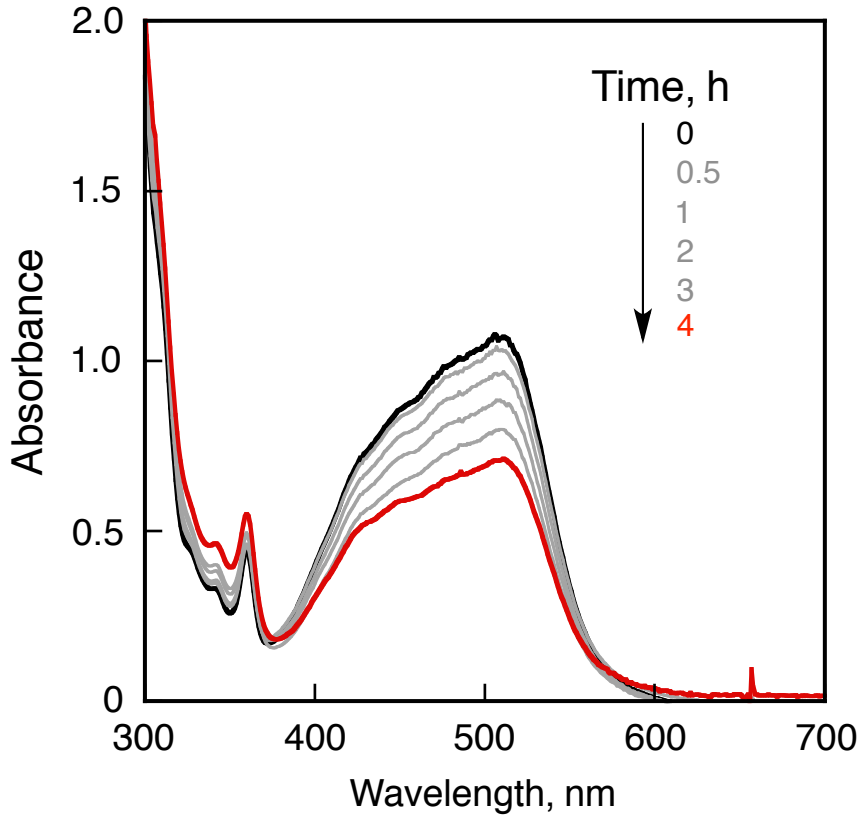

Fig. S3 Visible absorption changes in oxidation of $[Fe^{II}(Clphen)_3]^{2+}(PF_6^-)_2$ (1.0 mM) by O_2 in O_2-saturated acetonitrile containing HOTf (0.10 M) in the presence of $[Acr^+–Mes](ClO_4^-)$ (0.20 mM) at 298 K under visible light irradiation using a xenon lamp with a cut filter (λ > 390 nm) for 0 h (black line) and 4 h (red line).

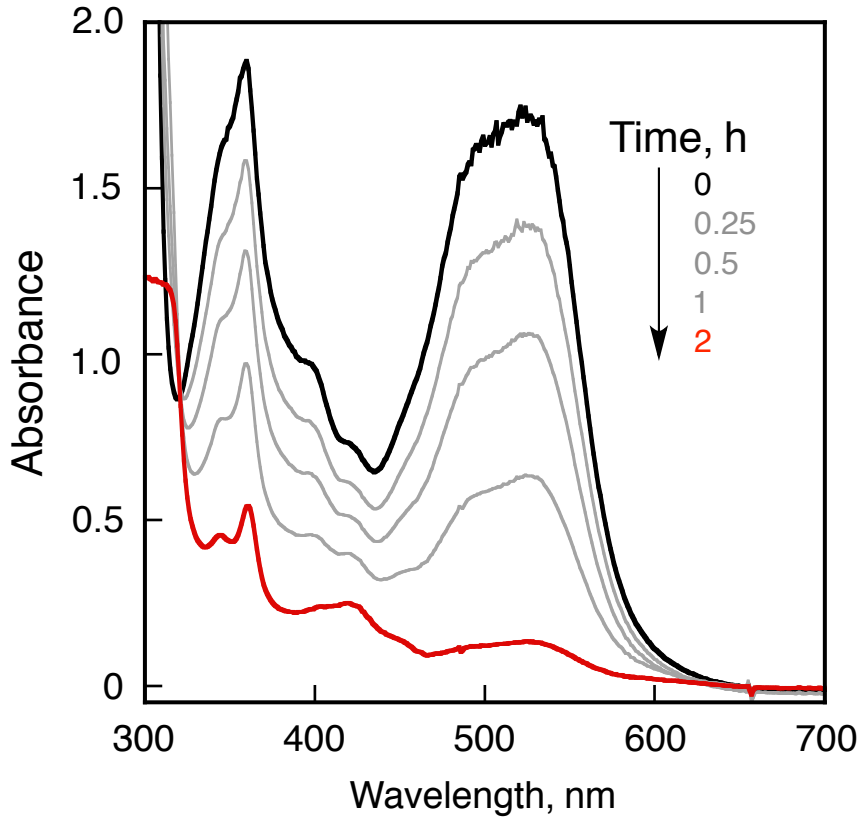

Fig. S4 Visible absorption changes in oxidation of $[Fe^{II}(Me_2bpy)_3]^{2+}(PF_6^-)_2$ (2.0 mM) by O_2 in O_2-saturated acetonitrile containing HOTf (0.10 M) in the presence of $[Acr^+–Mes](ClO_4^-)$ (0.20 mM) at 298 K under visible light irradiation using a xenon lamp with a cut filter ($\lambda >$ 390 nm) for 0 h (black line) and 2 h (red line).

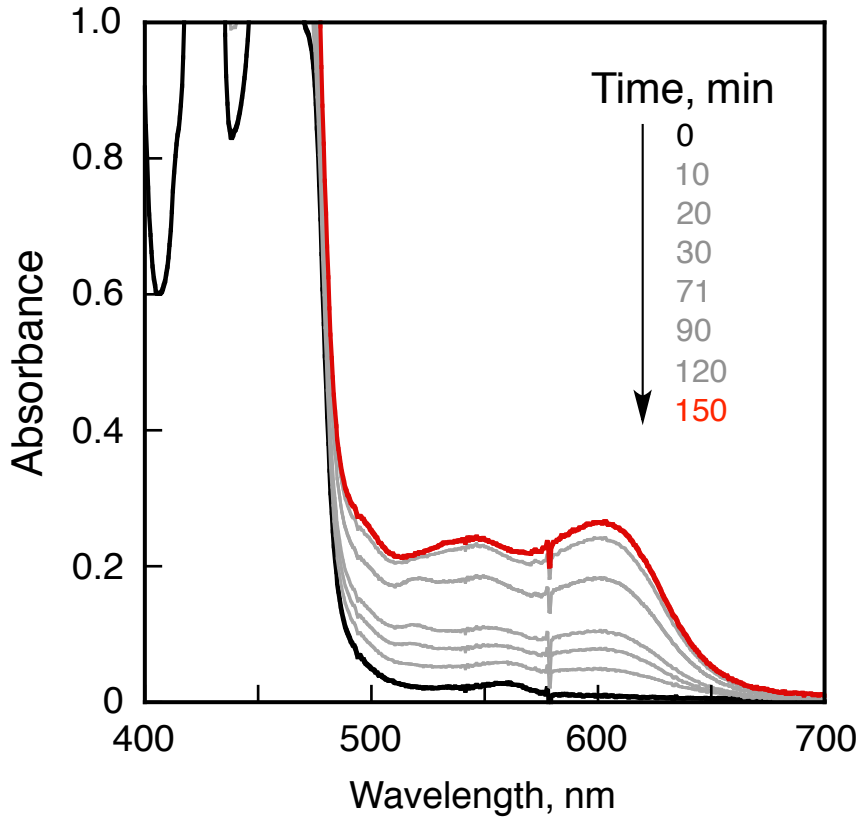

Fig. S5 Visible absorption changes in oxidation of $Fe^{II}(BrC_5H_4)_2$ (1.0 mM) by O_2 in O_2-saturated acetonitrile containing HOTf (0.10 M) in the presence of $[Acr^+–Mes](ClO_4^-)$ (0.20 mM) and at 298 K under visible light irradiation using a xenon lamp attached with a cut filter (λ > 390 nm) for 0 min (black line) and 150 min (red line).

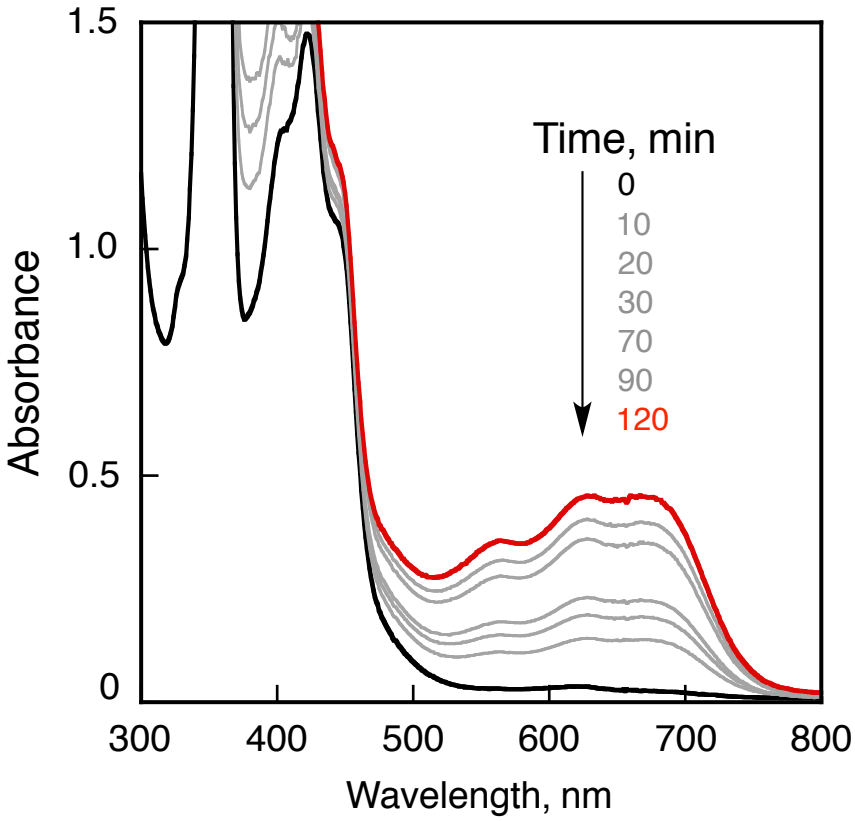

Fig. S6 Visible absorption changes in oxidation of $Fe^{II}(BrC_5H_4)(C_5H_5)$ (2.0 mM) by O_2 in O_2-saturated acetonitrile containing HOTf (0.10 M) in the presence of $[Acr^+–Mes](ClO_4^-)$ (0.20 mM) and at 298 K under visible light irradiation using a xenon lamp attached with a cut filter (λ > 390 nm) for 0 min (black line) and 120 min (red line).

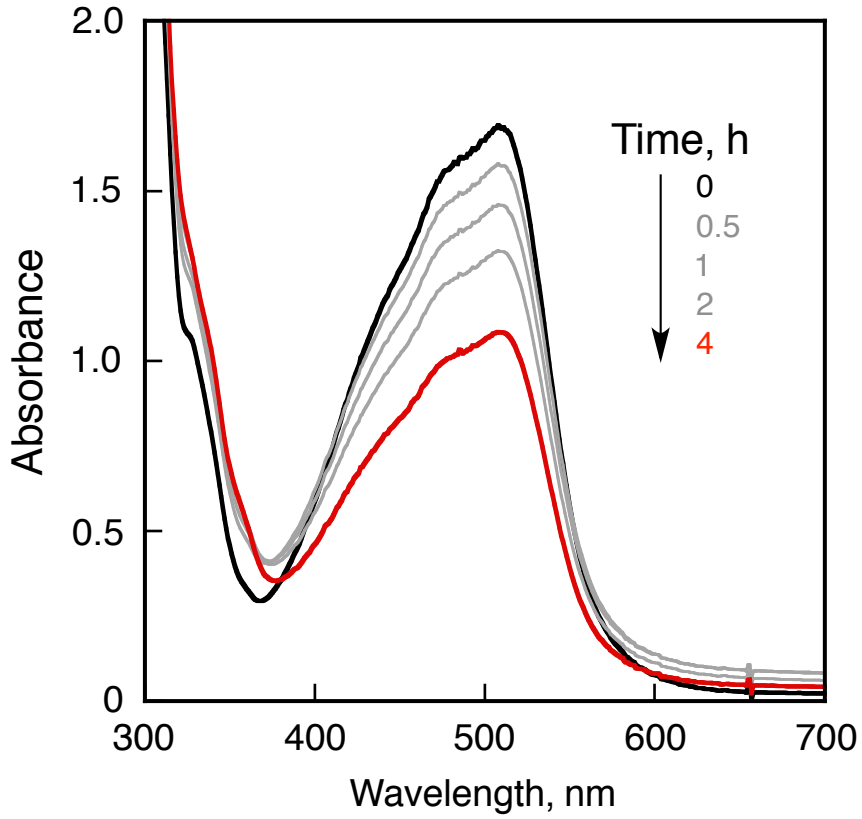

Fig. S7 Visible absorption changes in oxidation of $[Fe^{II}(Clphen)_3]^{2+}(PF_6^-)_2$ (1.5 mM) by O_2 in O_2-saturated acetonitrile containing HOTf (0.10 M) in the presence of $[QuPh^+–NA](ClO_4^-)$ (0.20 mM) at 298 K under visible light irradiation using a xenon lamp with a cut filter (λ > 300 nm) for 0 h (black line) and 4 h (red line).

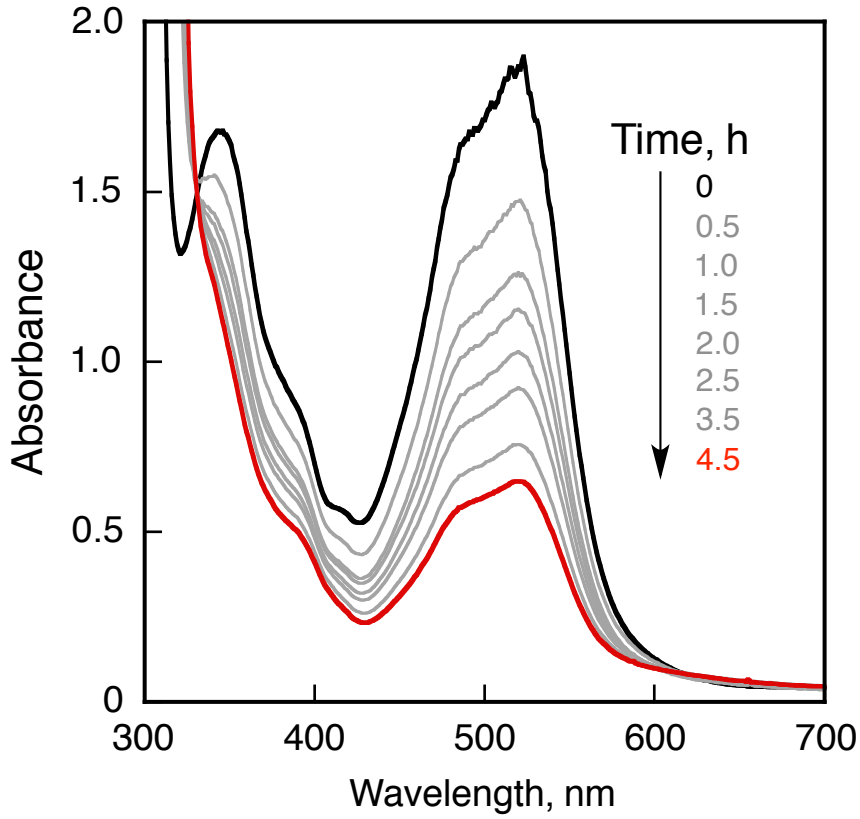

Fig. S8 Visible absorption changes in oxidation of $[Fe^{II}(bpy)_3]^{2+}(PF_6^-)_2$ (2.0 mM) by O_2 in O_2-saturated acetonitrile containing HOTf (0.10 M) in the presence of $[QuPh^+–NA](ClO_4^-)$ (0.20 mM) at 298 K under visible light irradiation using a xenon lamp with a cut filter (λ > 300 nm) for 0 h (black line) and 4.5 h (red line).

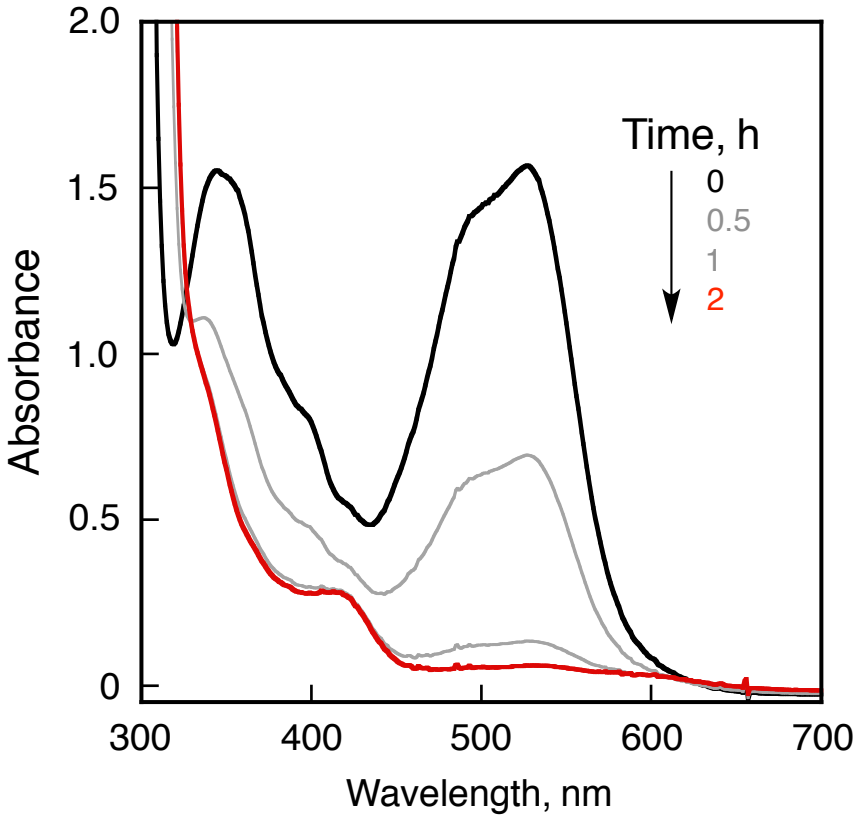

Fig. S9 Visible absorption changes in oxidation of $[Fe^{II}(Me_2bpy)_3]^{2+}(PF_6^-)_2$ (2.0 mM) by O_2 in O_2-saturated acetonitrile containing HOTf (0.10 M) in the presence of $[QuPh^+–NA](ClO_4^-)$ (0.20 mM) and at 298 K under visible light irradiation using a xenon lamp attached with a cut filter (λ > 300 nm) for 0 h (black line) and 2 h (red line).

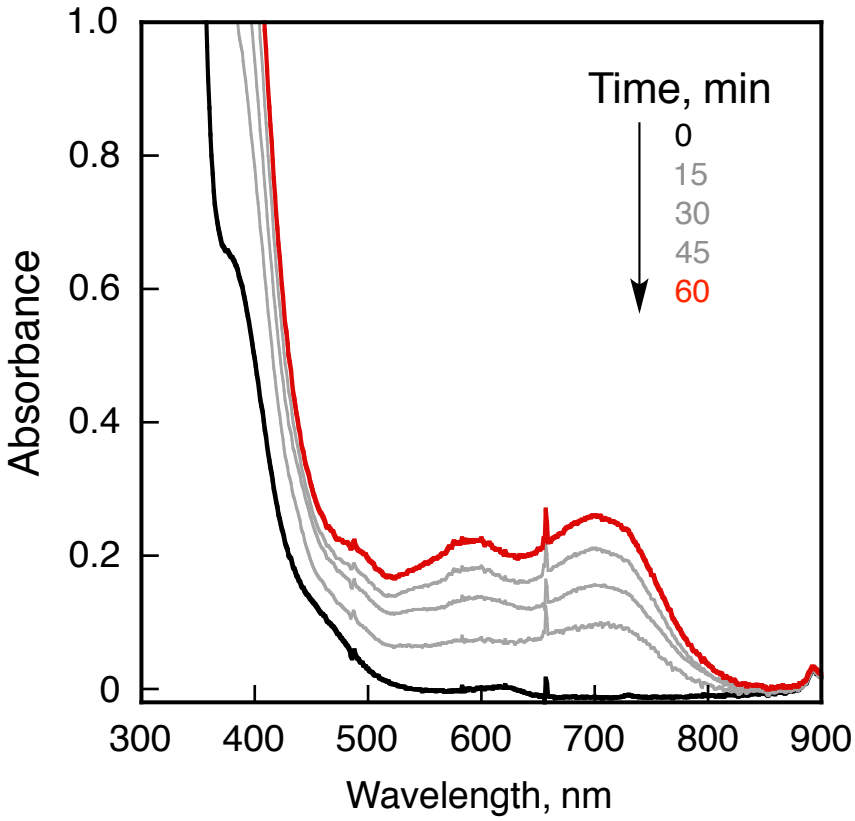

Fig. S10 Visible absorption changes in oxidation of $Fe^{II}(BrC_5H_4)_2$ (1.0 mM) by O_2 in O_2-saturated acetonitrile containing HOTf (0.10 M) in the presence of $[QuPh^+–NA](ClO_4^-)$ (0.20 mM) and at 298 K under visible light irradiation using a xenon lamp attached with a cut filter (λ > 300 nm) for 0 min (black line) and 60 min (red line).

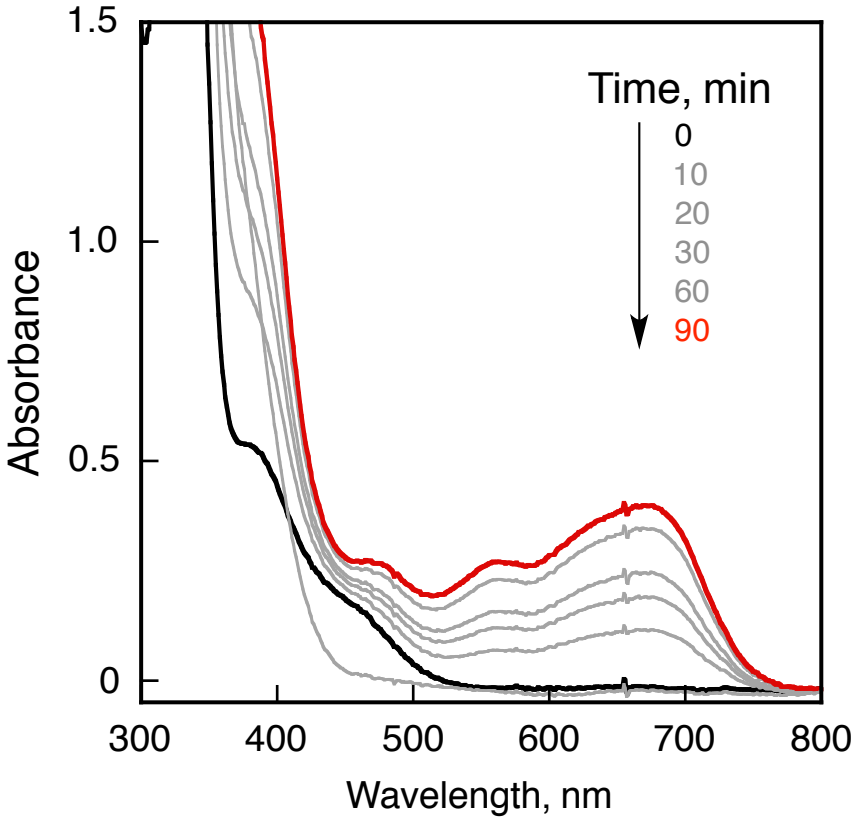

Fig. S11 Visible absorption changes in oxidation of $Fe^{II}(BrC_5H_4)(C_5H_5)$ (2.0 mM) by O_2 in O_2-saturated acetonitrile containing HOTf (0.10 M) in the presence of $[QuPh^+–NA](ClO_4^-)$ (0.20 mM) at 298 K under visible light irradiation using a xenon lamp attached with a cut filter (λ > 300 nm) for 0 min (black line) and 90 min (red line).

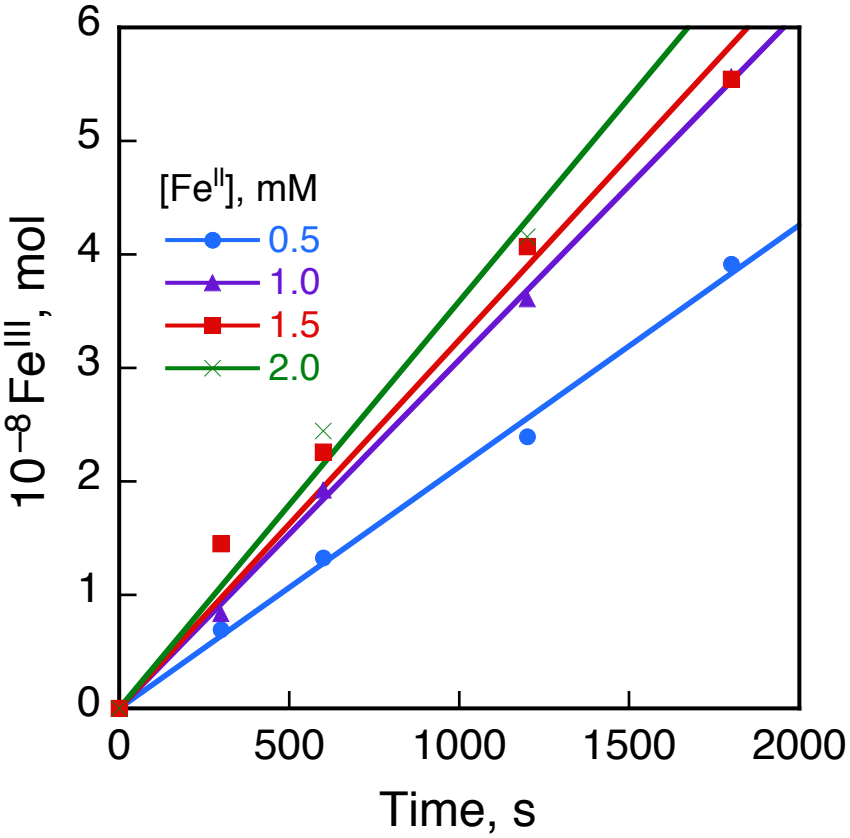

Fig. S12 Time course of Fe^{III} production at different concentrations of $[Fe^{II}(bpy)_3]^{2+}$ (PF_6^-) under monochromatized light (λ = 420 nm) irradiation in the presence of $[Acr^+–Mes](ClO_4^-)$ (1.0 mM) in acetonitrile (0.40 mL, $[O_2]$ = 2.6 mM) containing HOTf (0.15 M).

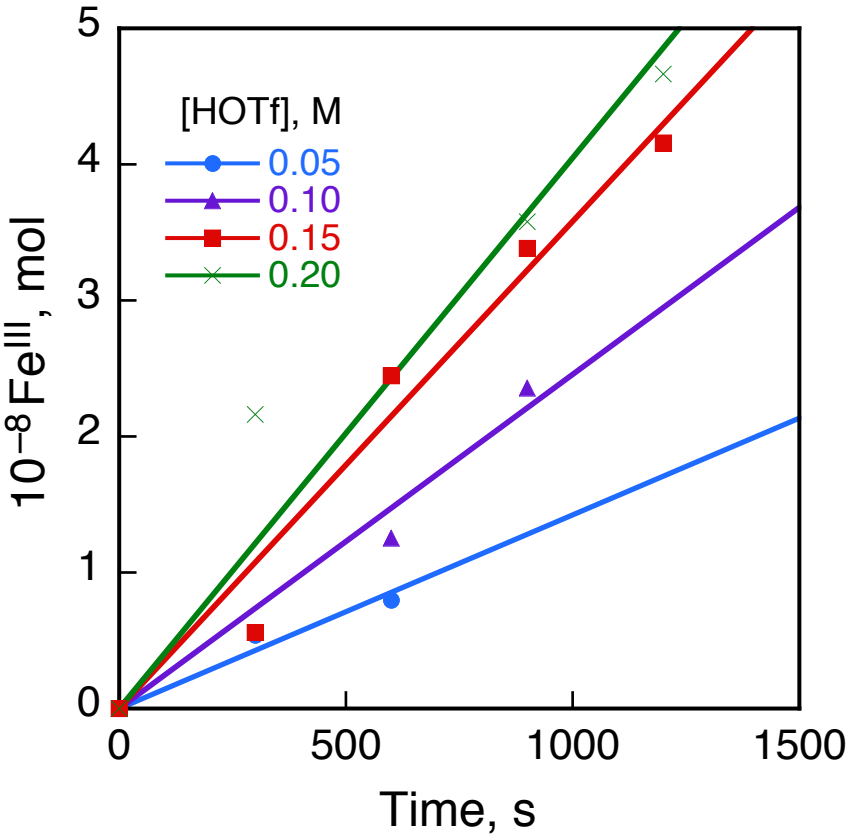

Fig. S13 Time course of Fe^{III} production at different concentrations of HOTf under monochromatized light (λ = 420 nm) irradiation in the presence of [Acr^{+}–Mes](ClO_4^{-}) (1.0 mM) in acetonitrile (0.40 mL, [O_2] = 2.6 mM) containing $[Fe^{II}(bpy)_3]^{2+}(PF_6^{-})$ (2.0 mM).

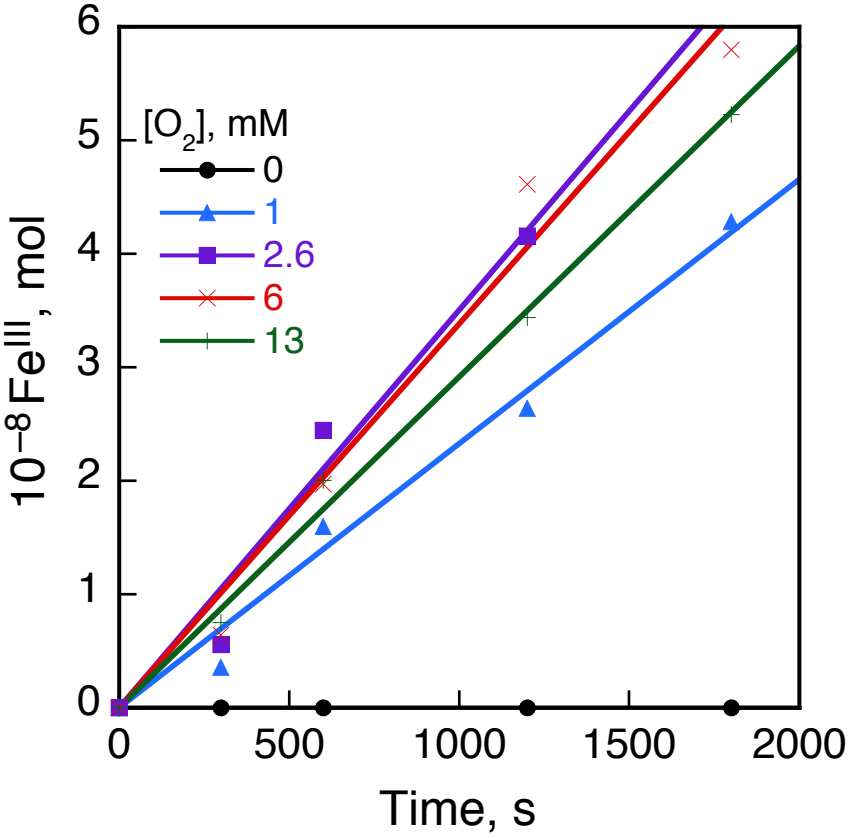

Fig. S14 Time course of Fe^{III} production at different concentrations of O_2 under monochromatized light (λ = 420 nm) irradiation in the presence of [Acr^{+}–Mes](ClO_4^{-}) (1.0 mM) in acetonitrile (0.40 mL) containing $[Fe^{II}(bpy)_3]^{2+}(PF_6^{-})$ (2.0 mM) and HOTf (0.15 M).

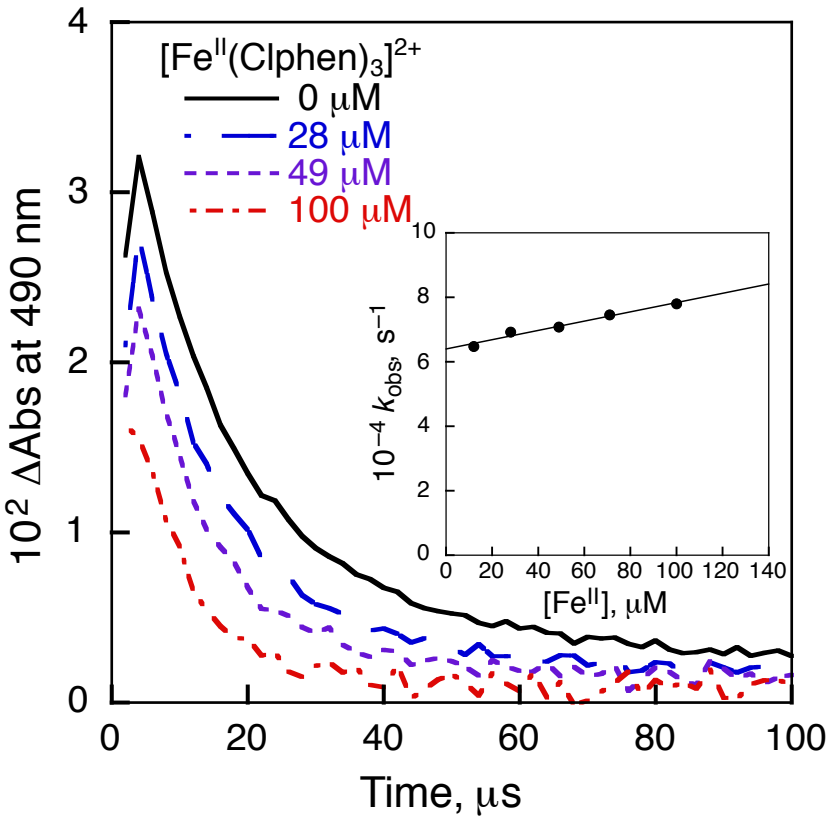

Fig. S15 Transient absorption decay at 490 nm due to the electron-transfer state of $[Acr^{+}–Mes](ClO_4^{-})$ with various concentrations of $[Fe^{II}(Clphen)_3]^{2+}(PF_6^{-})_2$. Inset: decay rate constant *versus* concentration of $[Fe^{II}(Clphen)_3]^{2+}(PF_6^{-})_2$.

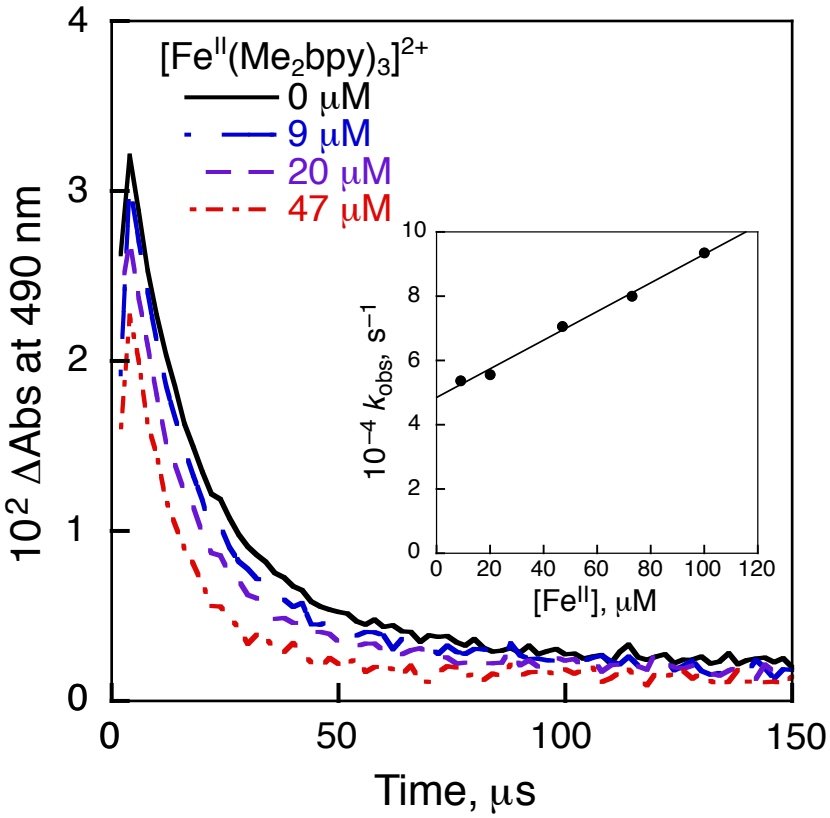

Fig. S16 Transient absorption decay at 490 nm due to the electron-transfer state of $[Acr^{+}–Mes](ClO_4^{-})$ with various concentrations of $[Fe^{II}(Me_2bpy)_3]^{2+}(PF_6^{-})_2$. Inset: decay rate constant *versus* concentration of $[Fe^{II}(Me_2bpy)_3]^{2+}(PF_6^{-})_2$.

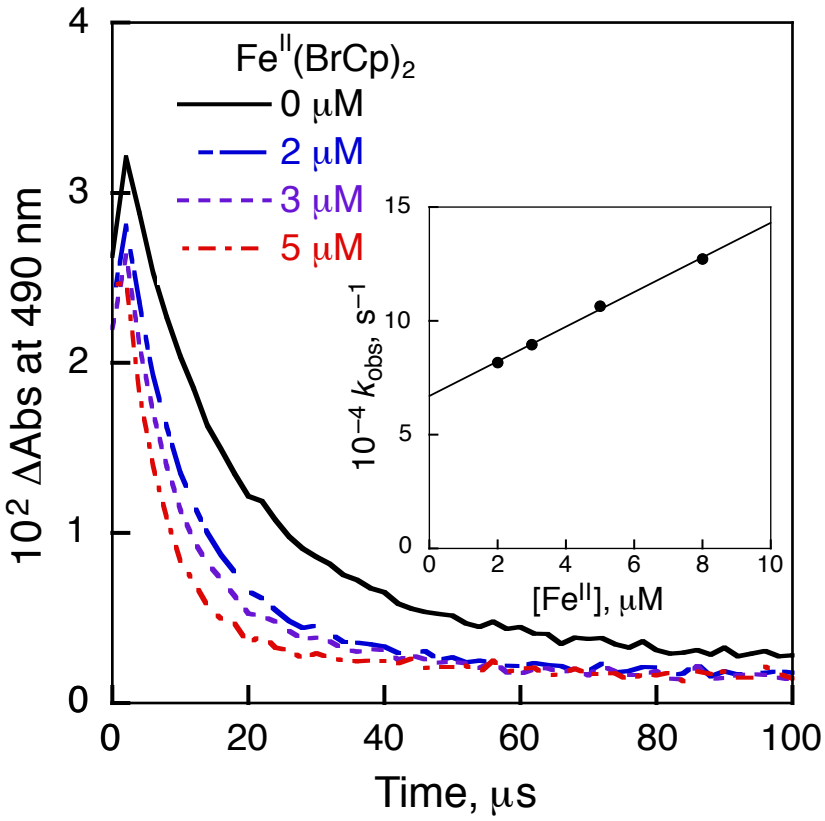

Fig. S17 Transient absorption decay at 490 nm due to the electron-transfer state of [Acr$^+$–Mes](ClO$_4^-$) with various concentrations of Fe^{II}(BrC$_5$H$_4$)$_2$. Inset: decay rate constant *versus* concentration of Fe^{II}(BrCp)$_2$.

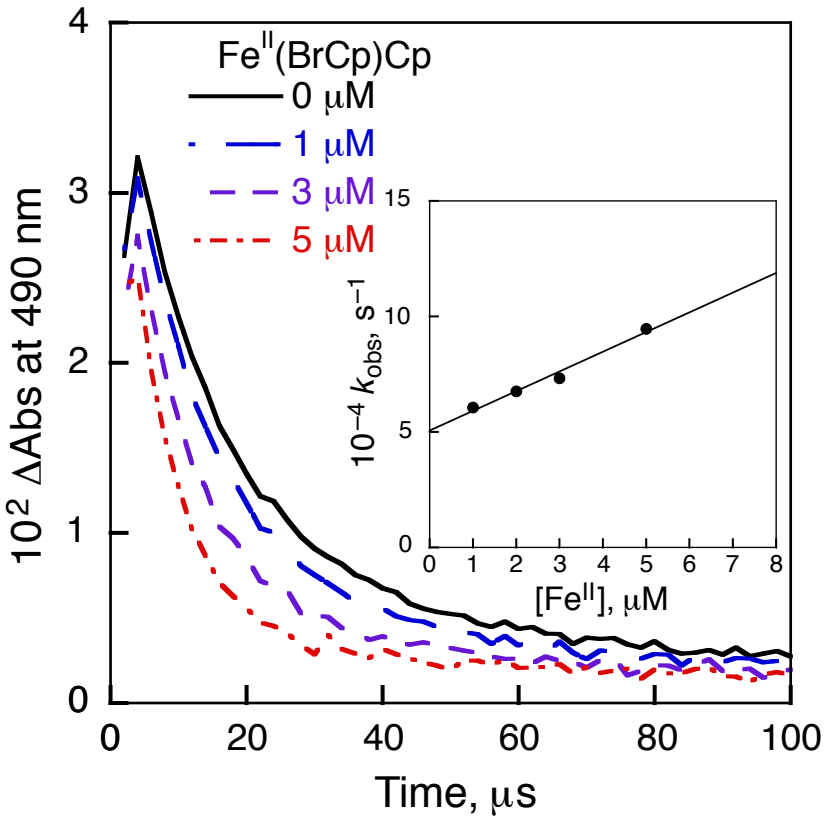

Fig. S18 Transient absorption decay at 490 nm due to the electron-transfer state of [Acr$^+$–Mes](ClO$_4^-$) with various concentrations of Fe^{II}(BrC$_5$H$_4$)(C$_5$H$_5$). Inset: decay rate constant *versus* concentration of Fe^{II}(BrCp)Cp.

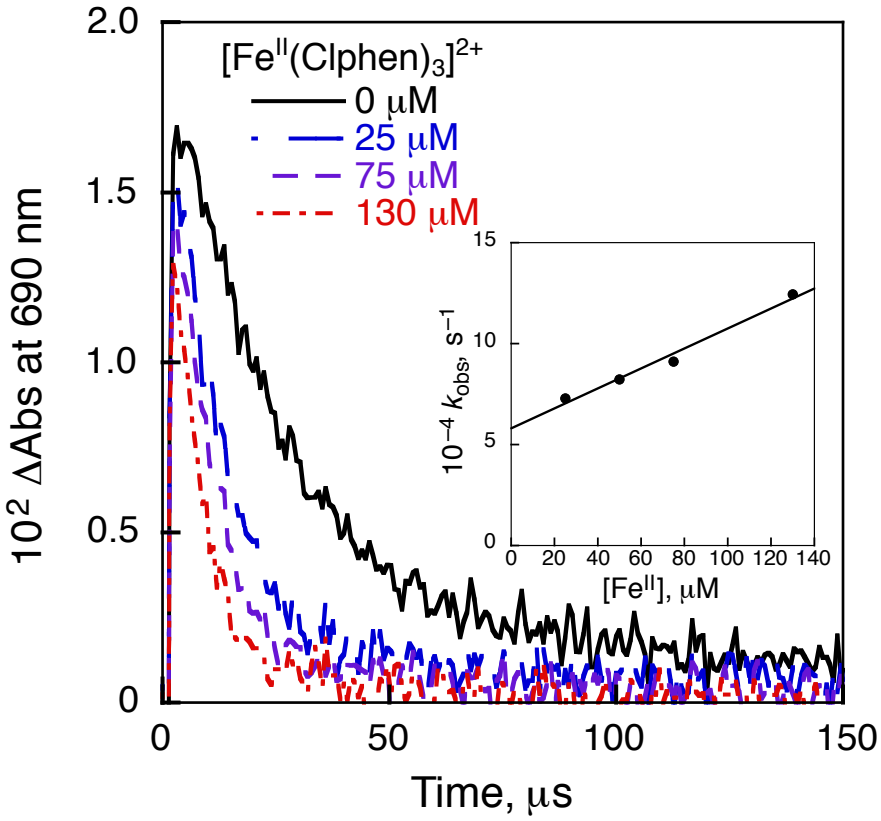

Fig. S19 Transient absorption decay at 690 nm due to the electron-transfer state of $[QuPh^{+}–NA](ClO_4^{-})$ with various concentrations of $[Fe^{II}(Clphen)_3]^{2+}(PF_6^{-})_2$. Inset: decay rate constant *versus* concentration of $[Fe^{II}(Clphen)_3]^{2+}(PF_6^{-})_2$.

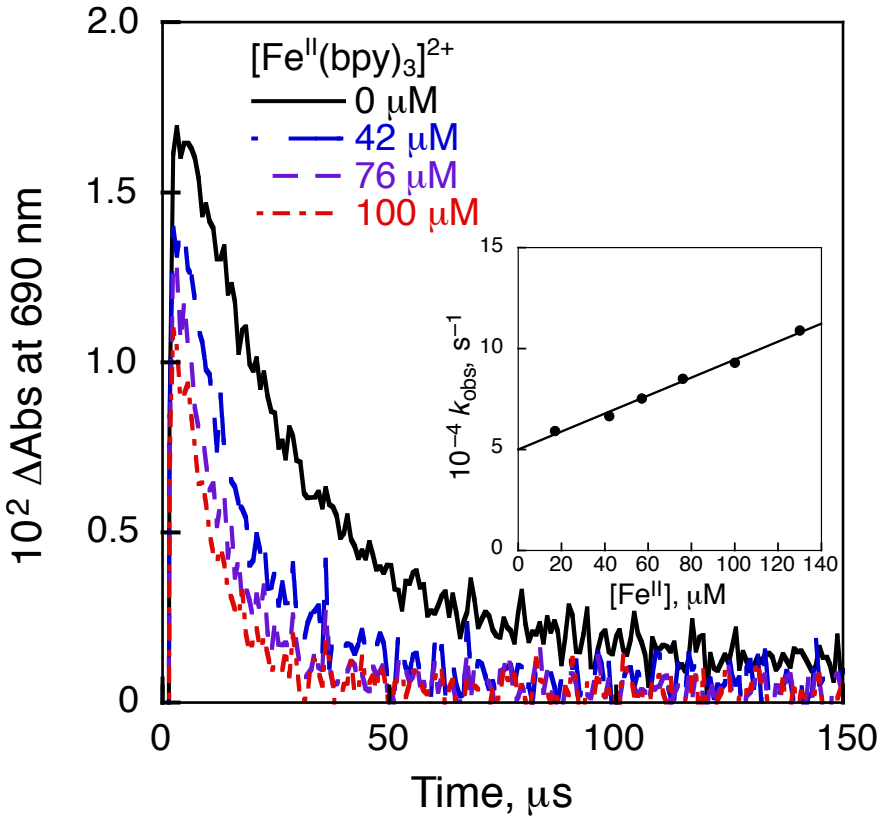

Fig. S20 Transient absorption decay at 690 nm due to the electron-transfer state of $[QuPh^{+}–NA](ClO_4^{-})$ with various concentrations of $[Fe^{II}(bpy)_3]^{2+}(PF_6^{-})_2$. Inset: decay rate constant *versus* concentration of $[Fe^{II}(bpy)_3]^{2+}(PF_6^{-})_2$.

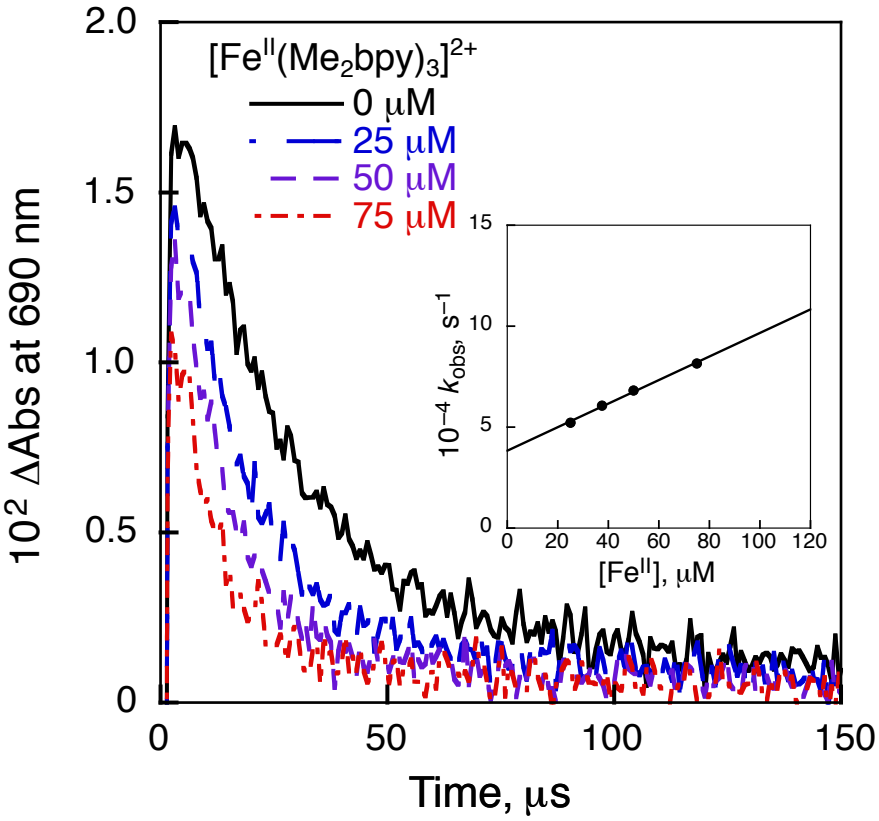

Fig. S21 Transient absorption decay at 690 nm due to the electron-transfer state of $[QuPh^{+}–NA](ClO_4^{-})$ with various concentrations of $[Fe^{II}(Me_2bpy)_3]^{2+}(PF_6^{-})_2$. Inset: decay rate constant *versus* concentration of $[Fe^{II}(Me_2bpy)_3]^{2+}(PF_6^{-})_2$.

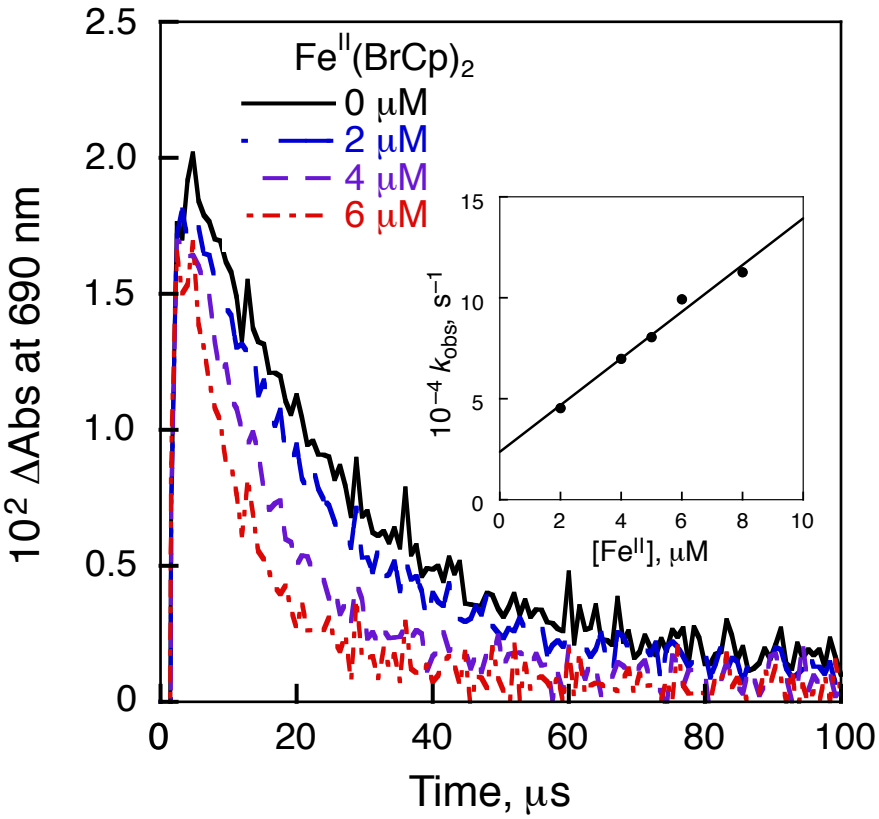

Fig. S22 Transient absorption decay at 690 nm due to the electron-transfer state of [QuPh$^+$–NA](ClO$_4^-$) with various concentrations of Fe^{II}(BrC$_5$H$_4$)(C$_5$H$_5$). Inset: decay rate constant *versus* concentration of Fe^{II}(BrCp)$_2$.

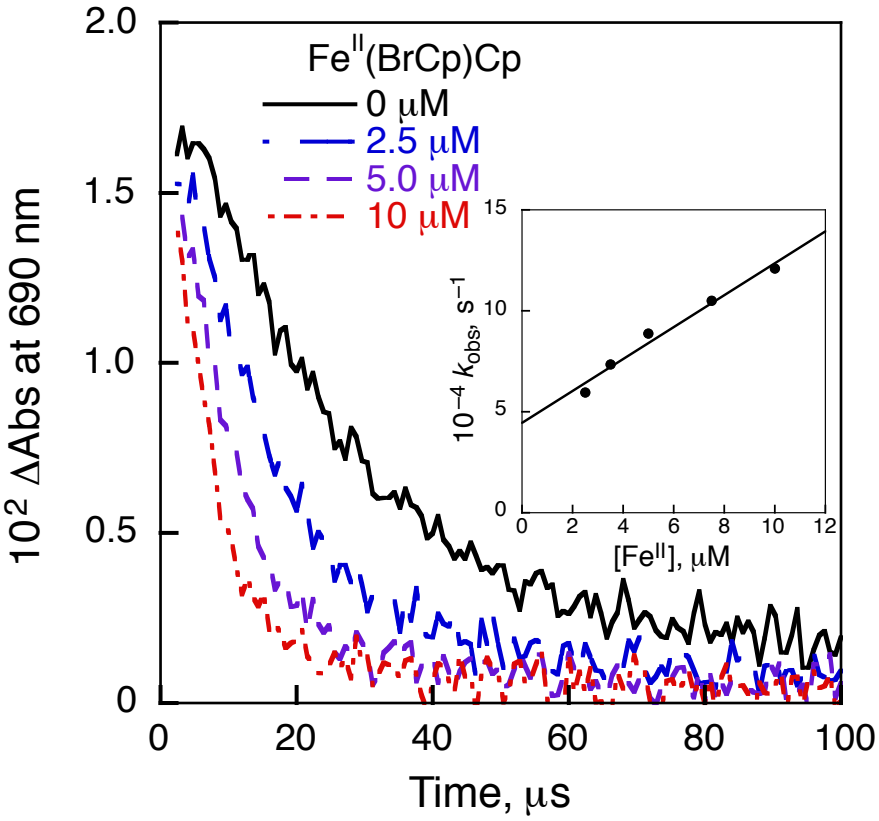

Fig. S23 Transient absorption decay at 690 nm due to the electron-transfer state of $[QuPh^{+}–NA](ClO_4^{-})$ with various concentrations of Fe^{II}(BrCp)Cp. Inset: decay rate constant versus concentrations of Fe^{II}(BrCp)Cp.

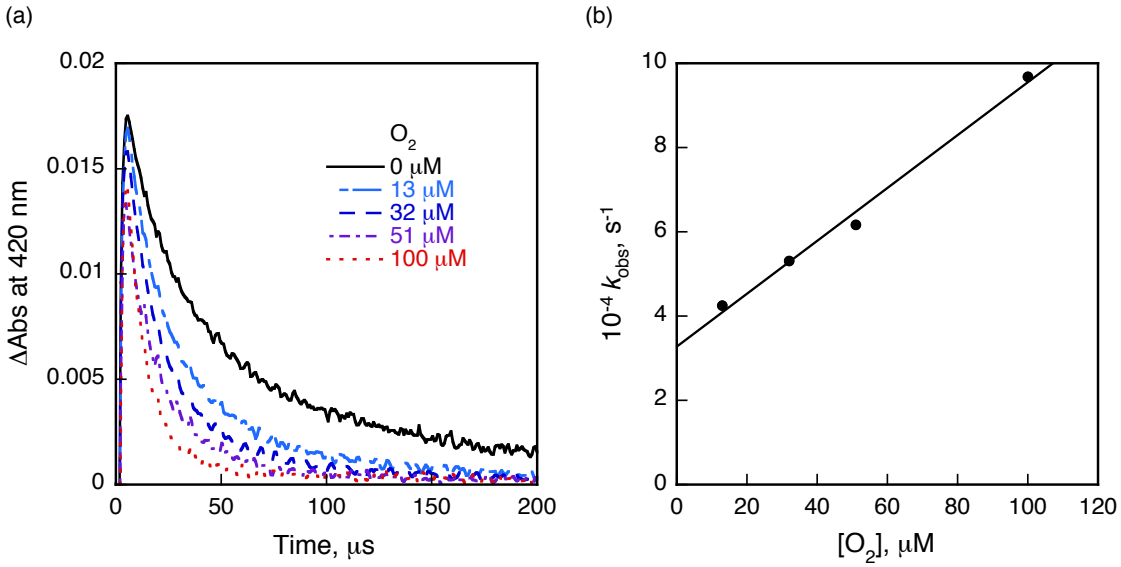

Fig. S24 (a) Transient absorption decay at 420 nm due to the electron-transfer state of [$QuPh^+$–NA](ClO_4^-) with various concentrations of O_2. (b) Decay rate constant *versus* concentration of O_2.